SELECTED PAPERS FROM IEEE ICCT 2023

Age of Loop Information with Flexible Transmission Enabled Communication and Control Co-Design in Industrial IoT

Chen Fangfang[1], Tang Jianhua[1,*], Yin Zihang[2]

[1] Shien-Ming Wu School of Intelligent Engineering, South China University of Technology, Guangzhou 511442, China
[2] China Academy of Information and Communications Technology, Beijing 100083, China
[*] The corresponding author, email: jtang4@e.ntu.edu.sg

Cite as: F. Chen, J. Tang, *et al*., "Age of loop information with flexible transmission enabled communication and control co-design in industrial iot," *China Communications*, 2024, vol. 21, no. 11, pp. 40-55. **DOI**: 10.23919/JCC.fa.2024-0218.202411

Abstract: Precise and low-latency information transmission through communication systems is essential in the Industrial Internet of Things (IIoT). However, in an industrial system, there is always a coupling relationship between the control and communication components. To improve the system's overall performance, exploring the co-design of communication and control systems is crucial. In this work, we propose a new metric – Age of Loop Information with Flexible Transmission (AoLI-FT), which dynamically adjusts the maximum number of uplink (UL) and downlink (DL) transmission rounds, thus enhancing reliability while ensuring timeliness. Our goal is to explore the relationship between AoLI-FT, reliability, and control convergence rate, and to design optimal blocklengths for UL and DL that achieve the desired control convergence rate. To address this issue, we first derive a closed-form expression for the upper bound of AoLI-FT. Subsequently, we establish a relationship between communication reliability and control convergence rates using a Lyapunov-like function. Finally, we introduce an iterative alternating algorithm to determine the optimal communication and control parameters. The numerical results demonstrate the significant performance advantages of our proposed communication and control co-design strategy in terms of latency and control cost.

Keywords: age of loop information; co-design; flexible transmission; IIoT

Received: May. 08, 2024
Revised: Jul. 20, 2024
Editor: Feng Wei

I. INTRODUCTION

The Industrial Internet of Things (IIoT) refers to the trend of applying Internet technology in the industrial sector, connecting various devices, sensors, and systems to collect, transmit, analyze, and apply data. The emergence of this technology has brought unprecedented changes and opportunities to industrial production [1]. In the IIoT, communication and control systems play crucial roles. The communication system is responsible for transmitting data collected from various devices and sensors to the central processing unit, while the control system implements corresponding control strategies based on this data to monitor and regulate the production process. However, designing relevant parameters to optimize the performance of both communication and control system to meet production demands remains a challenge.

In the modern industrial production process, the demand for precise control of equipment and efficient communication is increasingly prominent. The timeliness and reliability of the communication system play a decisive role in the response speed and stability of the control system [2]. Traditionally, however, communication systems and control systems are often designed and optimized separately, largely overlooking

the intrinsic connection and mutual influence between them. For instance, a communication system emphasizing reliability may not be suitable for control systems that require rapid response. The power industry utilizes remote monitoring to track the operational status of power transformers, enabling analysis and maintenance decisions. Similarly, the manufacturing industry monitors the operating conditions of production line equipment to detect and resolve equipment faults. These monitoring systems typically do not require immediate responses to the data but rely on reliable data transmission to support subsequent analysis and decision-making.

To balance the performance of communication and control systems, many scholars are dedicated to the research of sensing-communication-computing-control closed-loop optimization: (1) improving control performance as much as possible under the constraints of communication requirements, and (2) optimizing more realistic communication models given the desired control performance [3]. Presently, traditional communication metrics such as latency, throughput, and response time, along with control parameters like stability and convergence, are basically from individual domains, which do not fully reflect the performance characteristics of the integrated system [3]. On one hand, high efficiency in the communication system could lead to an overreaction in the control system. For communication systems that allow real-time data transmission, controllers can respond quickly. However, this may cause controllers to overreact to minor fluctuations or transient noise, affecting the system's stability and efficiency. For instance, in power distribution networks, data on load changes is frequently transmitted in real time. If there are transient fluctuations in the load, the controller might swiftly adjust the power distribution, even though these fluctuations might be temporary. Such frequent adjustments, however, increase the complexity and instability of the system. On the other hand, the stringent stability requirements of control systems may impose constraints on the performance of communication systems, such as the frequency of data transmission, latency tolerance, and redundancy mechanisms. For example, in a monitoring system, sensors measure data such as temperature and pressure and transmit the data to the controller via the communication system. The sensor data transmission is set to 1 Hz to ensure stable operation. However, this limitation reduces the real-time nature of the data. Therefore, designing a novel metric capable of assessing the performance of communication and control systems concurrently is essential to propel research in the co-design of these systems.

Traditional parameters that simultaneously influence control and communication systems mainly include sampling period, packet loss strategy, and transmission strategy [4–6]. For instance, applying an appropriate sampling period can achieve better control performance and reduce communication energy consumption. Based on the success of data transmission, wireless links can be added or removed to balance control stability and communication resource usage. However, considering the production demands in actual IIoT scenarios, there is an urgent need to establish new metrics that can comprehensively evaluate the combined performance of communication and control systems.

Currently, the emerging concept of Age of Information (AoI) and its extensions demonstrate unique advantages in optimizing communication performance, with the potential to drive the development of communication-control co-design. In our recent work, we proposed a novel metric – the Age of Loop Information (AoLI), which captures changes in data transmission time and transmission rounds in both the uplink (UL) and downlink (DL) processes. This metric aims to optimize the performance of both communication and control systems simultaneously [7]. Building upon this work, this paper further considers UL and DL wireless transmissions in multi-user scenarios and incorporates multiple antennas at the remote controller to enhance signal receiving quality. Moreover, this study dynamically allocates transmission attempts based on the success of UL and DL transmissions, improving reliability while ensuring the convergence rate of control. Our contributions of this work are:

1. We propose a new indicator, Age of Loop Information with Flexible Transmission (AoLI-FT), to measure the freshness of information in multi-user scenarios. This indicator can adaptively adjust the transmission rounds of both the uplink and downlink based on their channel conditions.

2. We derive a closed-form expression for the upper bound of the average AoLI-FT,which is a function of blocklength and average block error rate

in both uplink and downlink.

3. Using the proposed iterative search algorithm, we design the communication and control system parameters under control constraints to minimize AoLI-FT, achieving optimal synergy between the two.

II. RELATED WORKS

Several research works focus on balancing the performance of communication and control simultaneously. By increasing spectral efficiency and guaranteeing control convergence, [8] obtains the optimal optimization variable [3]. In [9], the authors create the optimal communication settings by reducing control and communication costs while adhering to communication limitations such maintaining the queue sequence's stability. Additionally, the authors in [10] create a combined framework for communication and control that relies on survival time. This refers to the duration a closed-loop wireless control system can operate without expecting a message. Furthermore, with less resource consumption, this framework can guarantee the stability of wireless control systems. Additionally, the authors in [11] proposed a unique distributed self-triggered control co-design technique for wireless multi-hop networks. The communication system allocates resources in accordance with the control system's advance notification of its transmission demands. Dynamic settings of both are required for various scenarios with diverse performance requirements for communication and control systems. Even though these approaches somewhat ensure optimal overall system performance, they must be tailored to specific needs. For example, communication performance may be suitably compromised in order to increase control convergence.

Recently, a new Quality of Service (QoS) metric known as the Age of Information (AoI) has been proposed to assess the timeliness and freshness of status updates [12], [13]. To better balance the performance of communication and control systems, [9] derived the relationship between control costs and the average AoI, and analyzed the correlation between average AoI and reliability, thereby confirming that AoI can measure both communication and control performance concurrently. However, the consideration of only the wireless transmission AoI from the sensor to the controller, with the assumption of ideal transmission from the controller to the actuator, has certain limitations. Further consideration is given to the fact that each of the aforementioned transmission mechanisms are wireless by [14] and [15]. One method shortens transmission duration using a state predictor, while another uses a finite Markov chain to model control information updates, resulting in the derivation of the average effective age of information (EAoI). This metric provides insights for designing efficient control systems. However, these approaches do not ensure communication system reliability. Examining the situation of machine type communication (MTC) state updates within the automatic repeat-request (ARQ) protocol, [16] investigates a method involving infinite re-transmissions, prioritizing reliability over transmission time. However, this approach may compromise control performance. Hence, there is a need to create a new metric that can balance the performance of control and communication.

III. SYSTEM MODEL

We examine a standard wireless communication-control system with M independent plants, as illustrated in Figure 1. Within each plant, multiple sensors and actuators are strategically deployed. The transmitter on the plant sends state packets to the remote controller via the uplink (UL). The remote controller generates the control commands based on the received states and sends them to the plant's receiver through the downlink (DL), which then actuates the actuators to control the factory. Each plant's transmitter is equipped with a single antenna, while the remote control system has L antennas. Consequently, the UL functions akin to a Single Input Multiple Output (SIMO) system, whereas the DL operates as a Multiple Input Single Output (MISO) system.

Additionally, assume that the state packet is transmitted at the start of the k-th sampling period. For the m-th plant, the state packet contains $\hat{I}_m$ bits of information, defined as $\boldsymbol{x}_{k,m} \in \mathbb{R}^{d_m}$ (d_m is the dimension of attributes of the m-th plant), which is encoded into $\hat{n}_m$ symbols through modulation, defined as $\hat{\boldsymbol{x}}_{k,m}$. Each symbol has a duration of T_s, and the bandwidth is $1/T_s$. The remote controller receives the modulated signal as $\hat{\boldsymbol{x}}'_{k,m}$ and demodulates it to $\boldsymbol{x}'_{k,m}$. Next, the controller computes the control command

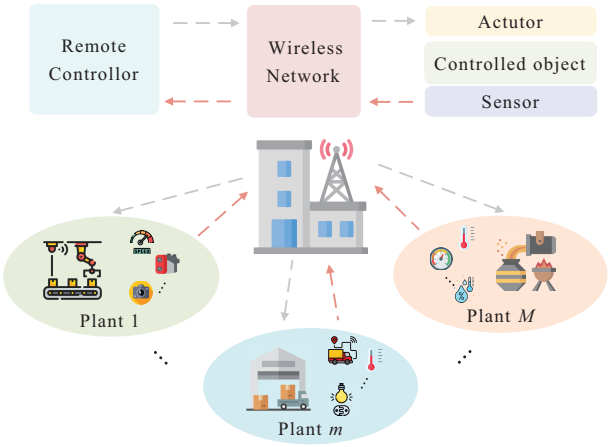

Figure 1. *System model.*

$\boldsymbol{u}_{k,m} \in \mathbb{R}^{q_m}$ (q_m is the control attribute dimension for the m-th plant), which contains $\breve{I}_m$ bits of information, and modulates it to $\breve{\boldsymbol{u}}_{k,m}$ with $\breve{n}_m$ symbols. After wireless transmission, the actuator receives the modulated control command $\breve{\boldsymbol{u}}'_{k,m}$ and demodulates it to obtain $\boldsymbol{u}'_{k,m}$.

3.1 Communication System Model

Received signal: After transmission through the wireless channel, the n-th information symbol of the m-th plant ($\hat{x}_{m,n}$) that is received by the controller can be written as [17]

$$\hat{x}'_{m,n} = \underbrace{\hat{\mathbf{w}}_m^H \hat{\mathbf{h}}_m \hat{x}_{m,n}}_{\text{desired signal}} + \underbrace{\sum_{i=1,i\neq m}^{M} \hat{\mathbf{w}}_m^H \hat{\mathbf{h}}_i \hat{x}_{m,i}}_{\text{interfering signal}} + \delta, \tag{1}$$

where $\hat{\mathbf{h}}_m \in \mathbb{C}^{L\times 1}$ corresponds to the channel vector from the m-th plant to the controller in the uplink, $\hat{\mathbf{w}}_m \in \mathbb{C}^{L\times 1}$ denotes the receive beamformer, and δ follows a Gaussian distribution with zero mean and variance σ^2, representing Additive White Gaussian Noise (AWGN).

The signal-to-interference-plus-noise ratio (SINR) at the controller from the m-th plant can be expressed as

$$\hat{\gamma}_m = \frac{\left|\hat{\mathbf{w}}_m^H \hat{\mathbf{h}}_m\right|^2}{\sum_{i=1,i\neq m}^{M} \left|\hat{\mathbf{w}}_m^H \hat{\mathbf{h}}_i\right|^2 + \sigma^2}. \tag{2}$$

In the DL, the SINR at the q-th actutor is [18]

$$\breve{\gamma}_q = \frac{\left|\breve{\mathbf{h}}_q^H \breve{\mathbf{w}}_q\right|^2}{\sum_{j=1,j\neq q}^{Q} \left|\breve{\mathbf{h}}_q^H \breve{\mathbf{w}}_j\right|^2 + \sigma^2}, \tag{3}$$

where $\breve{\mathbf{h}}_q \in \mathbb{C}^{L\times 1}$ corresponds to the channel vector from the controller to the q-th actuator, and $\breve{\mathbf{w}}_q \in \mathbb{C}^{L\times 1}$ represents the transmit beamformer for the q-th actuator (in the downlink).

Block Error Rate: The majority of data in IIoT scenarios, such as sensor data monitoring and device status monitoring, are sent in short packets. Therefore, the Shannon capacity cannot be used to capture the achievable transmission rate. For instance, in UL transmission, the finite blocklength capacity can be used to represent the achievable transmission rate as [8]

$$\hat{R}_m \approx \log(1+\hat{\gamma}_m) - \sqrt{\frac{\hat{V}_m}{\hat{n}_m}} Q^{-1}(\hat{\varepsilon}_m), \tag{4}$$

where $\hat{V}_m = 1 - \frac{1}{(1+\hat{\gamma}_m)^2}$ represents the channel dispersion. The inverse Gaussian Q-function is denoted by $Q^{-1}(\cdot)$, and the block error rate is represented by $\hat{\varepsilon}_m$, which is given by the following terms:

$$\begin{aligned}\hat{\varepsilon}_m &\approx Q\left(\frac{\sqrt{\hat{n}_m}\left(\log(1+\hat{\gamma}_m) - \frac{\hat{I}_m}{\hat{n}_m}\right)}{\sqrt{1-\frac{1}{(1+\hat{\gamma}_m)^2}}}\right) \\ &\approx \begin{cases} 1, & \hat{\gamma}_m < \hat{\delta}_m + 1/(2\hat{\alpha}_m), \\ \hat{\alpha}_m(\hat{\gamma}_m - \hat{\delta}_m) + 1/2, & \text{other}, \\ 0, & \hat{\gamma}_m > \hat{\delta}_m - (2\hat{\alpha}_m), \end{cases}\end{aligned} \tag{5}$$

where $\hat{\delta}_m = e^{\frac{\hat{I}_m}{\hat{n}_m}} - 1$, and $\hat{\alpha}_m = -\sqrt{\frac{\hat{n}_m}{2\pi\left(e^{2\hat{I}_m/\hat{n}_m}-1\right)}}$. I represents the amount of information bits, and $\hat{R}_m = \frac{\hat{I}_m}{\hat{n}_m}$. The Q function can be approximated as a linear function to obtain Eq. (5) [19].

3.2 Control System Model

System Model: At time instant k, the discrete time control function of the m-th plant is as follows [8]:

$$\boldsymbol{x}_{k+1,m} = \boldsymbol{\Phi}_m \boldsymbol{x}_{k,m} + \boldsymbol{\Gamma}^k_{0,m} \boldsymbol{u}'_{k,m} + \boldsymbol{\Gamma}^k_{1,m} \boldsymbol{u}'_{k-1,m} + \boldsymbol{v}_{k,m}, \tag{6}$$

where $\boldsymbol{\Phi}_m = e^{\mathbf{A}_m s}, \boldsymbol{\Gamma}^k_{0,m} = \int_0^{s-\tau_{k,m}} e^{\mathbf{A}_m t} \mathbf{B}_m dt$ and $\boldsymbol{\Gamma}^k_{1,m} = e^{\mathbf{A}_m (s-\tau_{k,m})} \int_0^{\tau_{k,m}} e^{\mathbf{A}_m t} \mathbf{B}_m dt$, where the sample period length is denoted by s. The transmission duration and idle duration of the k-th sample period (including UL and DL) are denoted as $[0,\ \tau_{k,m}]$ and $[\tau_{k,m},\ s]$, respectively. Additionally, the system matrix is represented by $\mathbf{A}_m \in \mathbb{R}^{d_m \times d_m}$ and the input matrix is represented by $\mathbf{B}_m \in \mathbb{R}^{d_m \times q_m}$. Besides, the Gaussian random system noise[1] with zero mean and covariance $\mathbf{V}_m \in \mathbb{R}^{d_m \times d_m}$ is represented as $\boldsymbol{v}_{k,m} \in \mathbb{R}^{d_m}$.

Due to imperfections in wireless transmission, packet loss may occur in both the uplink and downlink. It is assumed that successful DL transmission depends on the success of the UL transmission. In the m-th plant, let $\hat{\beta}_{k,m} = 1$ and $\breve{\beta}_{k,m} = 1$ respectively indicate that UL and DL transmissions are successful. Otherwise, set $\hat{\beta}_{k,m} = 0$ and $\breve{\beta}_{k,m} = 0$. We implement a linear feedback system for the controller, represented as $\boldsymbol{u}_{k,m} = -\boldsymbol{\Theta}_{k,m} \boldsymbol{\zeta}_{k,m}$, where $\boldsymbol{\Theta}_{k,m} \in \mathbb{R}^{q_m \times (d_m + q_m)}$ denotes the control gain. After a successful transmission, $\boldsymbol{u}'_{k,m} = \boldsymbol{u}_{k,m}$. Subsequently, we introduce the generalized state $\boldsymbol{\zeta}_{k,m} = \left[\boldsymbol{x}_{k,m};\ \boldsymbol{u}'_{k-1,m}\right]$ for the subsequent analysis. The closed-loop system can then be rewritten as

$$\boldsymbol{\zeta}_{k+1,m} = \begin{cases} \boldsymbol{\Psi}_m(s, \tau_{k,m}) \boldsymbol{\zeta}_{k,m} + \boldsymbol{\Omega}_m(s, \tau_{k,m}) \boldsymbol{u}'_{k,m} \\ \qquad\qquad + \overline{\boldsymbol{v}}_{k,m}, \\ \boldsymbol{\Psi}_m(\tau_{k,m}) \boldsymbol{\zeta}_{k,m} + \overline{\boldsymbol{v}}_{k,m}, \end{cases} \tag{7}$$

where $\boldsymbol{\Psi}_m(s, \tau_{k,m}) = \begin{bmatrix} \boldsymbol{\Phi}_m & \boldsymbol{\Gamma}^k_{1,m} \\ \boldsymbol{O_1} & \boldsymbol{O_2} \end{bmatrix}$, $\boldsymbol{\Omega}_m(s, \tau_{k,m}) = \begin{bmatrix} \boldsymbol{\Gamma}^k_{0,m} \\ \boldsymbol{I} \end{bmatrix}$ and $\overline{\boldsymbol{v}}_{k,m} = [\boldsymbol{v}_{k,m};\ \boldsymbol{O_3}]$. The zero matrices $\boldsymbol{O_1}$, $\boldsymbol{O_2}$, and $\boldsymbol{O_3}$ have dimensions $q \times d$, $q \times q$, and $q \times 1$, respectively. Additionally, $\boldsymbol{I}$ represents the identity matrix of size $q \times q$. Eq. (7) shows the calculation of $\boldsymbol{\zeta}_{k+1,m}$ for the case when $\hat{\beta}_{k,m}\breve{\beta}_{k,m} = 1$ and for other cases. A more generic form can be obtained by letting $\bar{\boldsymbol{\Psi}}_m(s, \tau_k) = \boldsymbol{\Psi}_m(s, \tau_k) - \boldsymbol{\Omega}_m(s, \tau_k) \boldsymbol{\Theta}_{k,m}$.

Control Performance: The control convergence rate in system design determines how quickly the system response reaches a steady state. It significantly impacts the system's dynamic performance, including real-time responsiveness, stability, and accuracy. Tailoring the convergence rate to specific application scenarios allows us to meet targeted performance indicators effectively.

Firstly, we focus on a Lyapunov-like function to determine the suitable control convergence rate:

$$L\left(\boldsymbol{\zeta}_{k,m}\right) = \boldsymbol{\zeta}^T_{k,m} \boldsymbol{R}_m \boldsymbol{\zeta}_{k,m}, \tag{8}$$

where $\boldsymbol{R}_m$ is a positive definite matrix. To reach the preset plant state, the Lyapunov function must meet the following requirements:

$$\mathbb{E}\left[L\left(\boldsymbol{\zeta}_{k+1,m}\right) \mid \boldsymbol{\zeta}_{k,m}\right] \leq \rho_m L\left(\boldsymbol{\zeta}_{k,m}\right) + \mathrm{Tr}\left(\boldsymbol{R}_m \overline{\boldsymbol{V}}_m\right), \tag{9}$$

where ρ_m represents the control convergence rate, and $\overline{\boldsymbol{V}}_m = [\boldsymbol{V}_m;\ \boldsymbol{O}_3]$. The convergence of the control system is ensured by maintaining rates $\rho_m < 1$ [20].

Control Cost: We use the linear quadratic regulator (LQR) control cost to assess control performance. This cost is determined by [21]

$$J_m = \mathbb{E}\left[\sum_{k=0}^{K-1} \left(\boldsymbol{\zeta}^T_{k,m} \mathbf{G}_m \boldsymbol{\zeta}_{k,m} + {\boldsymbol{u}'_{k,m}}^T \mathbf{U}_m \boldsymbol{u}'_{k,m}\right) + \boldsymbol{\zeta}^T_{K,m} \mathbf{G}_m \boldsymbol{\zeta}_{K,m}\right], \tag{10}$$

where $\mathbf{G}_m$ and $\mathbf{U}_m$ are symmetric weighting matrices, with the former being positive semi-definite and the latter being positive definite. The variable K represents the number of update packets received by the actuator before time t.

Control Gain: The optimal control gain, which minimizes Eq. (10), is represented as described in [22]. To maintain brevity, the subscripts $(s, \tau_{k,m})$ of $\boldsymbol{\Omega}$ and $\boldsymbol{\Psi}$ are omitted in this representation.

$$\boldsymbol{\Theta}^*_{k,m} = \left(\mathbf{U}_m + \boldsymbol{\Omega}^T_m \bar{\mathbf{P}}_m \boldsymbol{\Omega}_m\right)^{-1} \boldsymbol{\Omega}^T_m \bar{\mathbf{P}}_m \boldsymbol{\Psi}_m, \tag{11}$$

where the steady-state solution of the control Riccati recursion, denoted as $\bar{\mathbf{P}}_m$, can be written as follows:

$$\bar{\mathbf{P}}_m = \boldsymbol{\Psi}^T_m \bar{\mathbf{P}}_m \boldsymbol{\Psi}_m - \boldsymbol{\Psi}^T_m \bar{\mathbf{P}}_m \boldsymbol{\Omega}_m \left(\boldsymbol{\Omega}^T_m \bar{\mathbf{P}}_m \boldsymbol{\Omega}_m + \boldsymbol{U}_m\right)^{-1} \times \boldsymbol{\Omega}^T_m \bar{\mathbf{P}}_m \boldsymbol{\Psi}_m + \boldsymbol{G}_m. \tag{12}$$

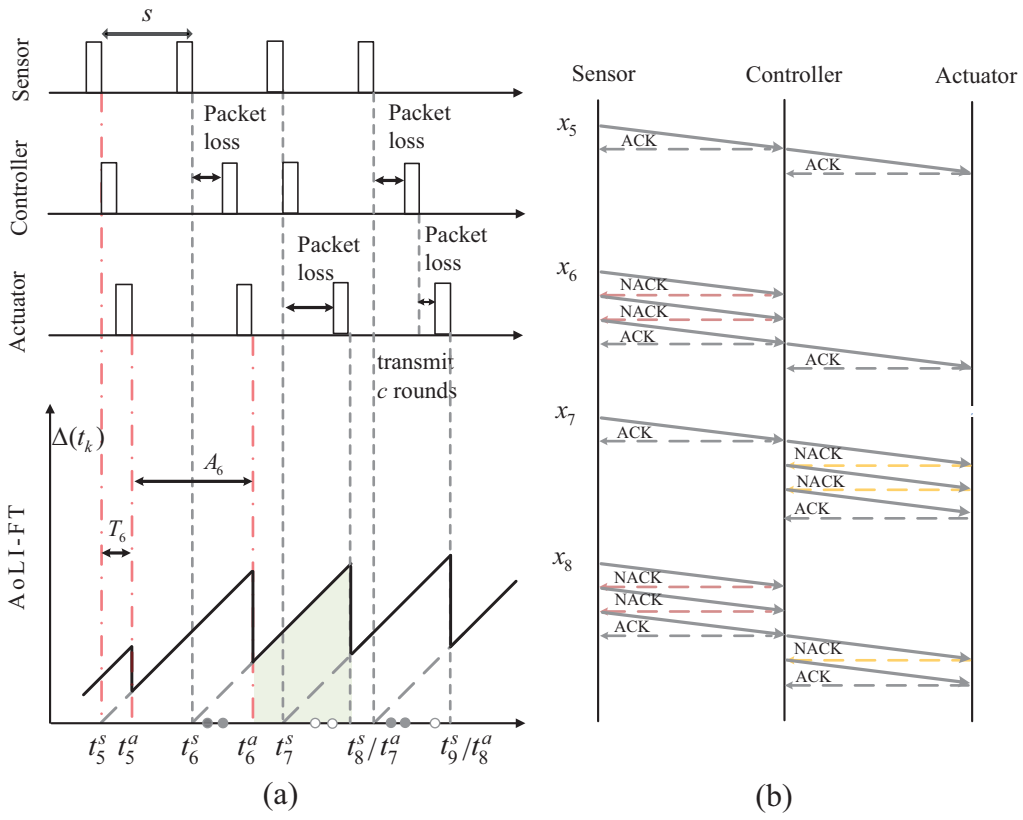

Figure 2. *UL and DL wireless transmission diagram. (a) The evolution of AoLI-FT. Solid circles represent transmission rounds for the UL, while hollow circles represent those for the DL. t_k^s indicates the generation of the k-th sample, while t_k^a indicates its successful reception. (b) Transmission process.*

3.3 Age of Loop Information with Flexible Transmission

Assuming that the transmission process of state packets follows the First-Come-First-Served service rule, we model this process as an $M/G/1$ queuing system. Status packets are generated based on a Poisson process with an average arrival rate of $\lambda = 1/s$. Next, we will discuss the expression for AoLI-FT for the case of a single plant and multiple plants respectively.

1) ***Case 1:*** Considering only one plant, $M = 1$.

Figure 2 shows the evolution process of AoLI-FT in this case. It can be seen that the status packet can be transmitted or retransmitted to the destination, with transmission rounds $\hat{c}$. Similarly, the control command in the downlink can also be transmitted or retransmitted ($\check{c}$ times) until successfully received by the actuator, under the condition of ensuring correct uplink transmission. Assuming that the number of transmission rounds for both the uplink and the downlink is c, and $\hat{c}+\check{c} \leq c$, successful transmission is guaranteed under the maximum number of c retransmissions. In addition, it is assumed that the destination will send an ACK or NACK message back to the sender after receiving the packet. The sender will send the most recent status packet again if it receives a NACK; otherwise, it will send the subsequent new status packet [23, 24].

As illustrated in Figure 2, during the k-th update process, the area under the AoLI-FT curve is denoted as S_k. The average AoLI-FT can be formally defined according to [16].

$$\begin{aligned}\bar{\Delta} &= \lim_{t\to\infty} \frac{1}{t} \sum_{k=1}^{K(t)} S_k \\ &= \frac{\tilde{\lambda}\left[\mathbb{E}\left(A^2\right) + 2\mathbb{E}(T)\mathbb{E}(A)\right]}{2},\end{aligned} \tag{13}$$

where $S_k = (A_k + 2T_k)\, A_k/2$, representing the shadow part of the trapezoid. $A_k = t_k^a - t_{k-1}^a$ and

$T_k = t^a_{k-1} - t^s_{k-1}$. Besides, $K(t)$ represents the cumulative number of update packets received by the destination before time t, and $\tilde{\lambda}$ denotes the average arrival rate of update packets, calculated as $\lim_{t\to\infty} \frac{K(t)}{t}$. Each packet's first-order moment of the sojourn time can be represented as $\mathbb{E}(T) = T_s(\mathbb{E}(\hat{C})\hat{n} + \mathbb{E}(\breve{C})\breve{n})$, where $\mathbb{E}(\hat{C})$ and $\mathbb{E}(\breve{C})$ represent the average rounds of transmissions for the UL and DL respectively. The average rate of information updates can be expressed as

$$\tilde{\lambda} = \frac{1}{\frac{1}{\lambda} + \mathbb{E}(T)}. \tag{14}$$

The expression for $\mathbb{E}(A)$ is as follows:

$$\mathbb{E}(A) = \sum_{i=1}^{c} \mathbb{E}(A \mid C = i)\mathbb{P}(C = i). \tag{15}$$

Similarly, we can obtain $\mathbb{E}(A^2)$ as

$$\mathbb{E}(A^2) = \sum_{j=1}^{c} \mathbb{E}(A^2 \mid C = j)\mathbb{P}(C = j). \tag{16}$$

*2) **Case 2:*** Considering M plants.

For M plants, the average AoLI-FT can be defined as follows:

$$\bar{\Delta}' = \frac{1}{M} \sum_{m\in\mathcal{M}} \bar{\Delta}_m, \tag{17}$$

where $\mathcal{M} = \{1, \ldots, M\}$ denote the set of plants.

3.4 Problem Formulation

In the scenario of M plants, $\boldsymbol{\rho} = [\rho_1, \rho_2, ..., \rho_M]$ represents the control convergence rate vector. $\hat{\boldsymbol{n}} = [\hat{n}_1, \hat{n}_2, ..., \hat{n}_M]$ and $\breve{\boldsymbol{n}} = [\breve{n}_1, \breve{n}_2, ..., \breve{n}_M]$ represent the blocklength vectors in the UL and DL transmission processes, respectively. As AoLI-FT can reflect both the control systems and communication systems [9], our goal is to minimize $\bar{\Delta}'$. Therefore, we define the following optimization problem:

$$\boldsymbol{Q1}: \min_{\boldsymbol{\rho},\hat{\boldsymbol{n}},\breve{\boldsymbol{n}},\hat{\mathbf{w}}_{k,m},\breve{\mathbf{w}}_{k,m}} \bar{\Delta}'$$

$$s.t. \ \frac{\hat{I}_{k,m}}{log_2\hat{\Theta}_m} \le \hat{n}_{k,m} \le \hat{n}_{\max}, \ \forall k, \tag{18a}$$

$$\frac{\breve{I}_{k,m}}{log_2\breve{\Theta}_m} \le \breve{n}_{k,m} \le \breve{n}_{\max}, \ \forall k, \tag{18b}$$

$$\sum_m \|\hat{\mathbf{w}}_{k,m}\|_2^2 \le \hat{P}_{\max}, \ \forall k, \tag{18c}$$

$$\sum_m \|\breve{\mathbf{w}}_{k,m}\|_2^2 \le \breve{P}_{\max}, \ \forall k, \tag{18d}$$

$$0 < \rho < 1, \tag{18e}$$

$$(9), \tag{18f}$$

where $\hat{\Theta}_m$ and $\breve{\Theta}_m$ represent the modulation schemes in the UL and DL of the m-th plant, respectively. $\hat{P}_{\max}$ and $\breve{P}_{\max}$ represent the maximum power in the UL and DL, respectively, and normally $\hat{P}_{\max} = 1$.

IV. MAIN RESULTS

Problem $\boldsymbol{Q1}$ is hard to tackle since the variables are deeply coupled. To make it more tractable, we first derive the receive/transmit beamformer.

In this paper, we use the Minimum Mean Square Error (MMSE) detector to construct $\hat{\mathbf{w}}_{k,m}$ (i.e., the receive beamformer) and $\breve{\mathbf{w}}_{k,m}$ (i.e., the transmit beamformer) as follows [25] [26]:

$$\mathbf{w}_m^T = \varpi \mathbf{w}'_m, \tag{19}$$

where $[\mathbf{w}'_m = \mathbf{h}_m^H \left(\mathbf{h}_m\mathbf{h}_m^H + \frac{\sigma^2}{P_{\max}}\mathbf{I}\right)^{-1}]$ and the introduction of $\varpi = \sqrt{\frac{P_{\max}}{\mathrm{Tr}(\mathbf{w}'^H_m \mathbf{w}'_m)}}$ is to satisfy the power constraints.

Once the receive/transmit beamformer is given by (19), problem $\boldsymbol{Q1}$ becomes finding the optimal ρ, $\hat{\boldsymbol{n}}$ and $\breve{\boldsymbol{n}}$ for m plants under the condition of minimizing AoLI-FT. According to (17), problem $\boldsymbol{Q1}$ can be then decomposed into finding the minimum AoI-FT for each plant. However, the problem remains intractable even when $M = 1$. Therefore, by establishing the upper bound of AoLI-FT, which adaptively adjusts the transmission rounds of the uplink and downlink, we simplify the problem and design an algorithm to find suitable optimization variables.

Theorem 1. *For a plant with finite re-transmission rounds, the upper bound of the average AoLI-FT is*

$$\hat{\Delta} = \mathbb{E}(\bar{A}) + \frac{0.5b_2}{s + \mathbb{E}(\bar{T})}, \tag{20}$$

where $b_2 = \mathbb{E}(\bar{A}^2) - 2s^2 - 2s(\mathbb{E}(\bar{A}) - s)$.

Proof. See Appendix A.

To explore the relationship between the control system and the communication system, we rewrite (9) based on [8] as follows:

$$p_{k,m} \geq \frac{\boldsymbol{\zeta}_{k,m}^T \left(\boldsymbol{\Psi}_m^T \mathbf{R}_m \boldsymbol{\Psi}_m - \rho_m \mathbf{R}_m \right) \boldsymbol{\zeta}_{k,m}}{\boldsymbol{\zeta}_{k,m}^T \left(\boldsymbol{\Psi}_m^T \mathbf{R}_m \boldsymbol{\Psi}_m - \bar{\boldsymbol{\Psi}}_m^T \mathbf{R}_m \bar{\boldsymbol{\Psi}}_m \right) \boldsymbol{\zeta}_{k,m}}, \tag{21}$$

where $p_{k,m} = (1-\hat{\varepsilon}_{k,m})(1-\breve{\varepsilon}_{k,m})$. According to [8], an upper bound for the right-hand side of Eq. (21) exists. By minimizing J to obtain $\rho_{\min}$, and substituting its steady state $\boldsymbol{\zeta}^*$ into Eq. (21), we can determine the lower bound of the inequality in Eq. (21).

Although state updates are correlated across different time indices k, the allocation of wireless resources required for control is independent. Additionally, resources such as transmission power are distinct across various plants. Consequently, we can eliminate the time index k and divide Problem $\boldsymbol{Q1}$ into M subproblems. Therefore, $\boldsymbol{Q1}$ can be rewritten as

$$\begin{aligned}
\boldsymbol{Q2}: \min_{\rho,\hat{n},\breve{n}} \ & \hat{\Delta} \\
s.t. \ & \frac{\hat{I}}{log_2 \hat{\Theta}} \leq \hat{n} \leq \hat{n}_{\max}, && \text{(22a)} \\
& \frac{\breve{I}}{log_2 \breve{\Theta}} \leq \breve{n} \leq \breve{n}_{\max}, && \text{(22b)} \\
& \|\hat{\mathbf{w}}\|_2^2 \leq \hat{P}_{\max}, && \text{(22c)} \\
& \|\breve{\mathbf{w}}\|_2^2 \leq \breve{P}_{\max}, && \text{(22d)} \\
& 0 < \rho < 1, && \text{(22e)} \\
& p = \frac{\boldsymbol{\zeta}^{*T} \left(\boldsymbol{\Psi}^T \mathbf{R} \boldsymbol{\Psi} - \rho \mathbf{R} \right) \boldsymbol{\zeta}^*}{\boldsymbol{\zeta}^{*T} \left(\boldsymbol{\Psi}^T \mathbf{R} \boldsymbol{\Psi} - \bar{\boldsymbol{\Psi}}^T \mathbf{R} \bar{\boldsymbol{\Psi}} \right) \boldsymbol{\zeta}^*}, && \text{(22f)}
\end{aligned}$$

where p represents the reliability, and $p = (1-\hat{\varepsilon})(1-\breve{\varepsilon})$. From Appendix B and C in [7], taking into account the requirements of real-world industrial scenarios, our primary focus lies on the condition $u < v$ (where $u = (\boldsymbol{\Psi}\boldsymbol{\zeta}^*)^T \mathbf{R} \boldsymbol{\Psi}\boldsymbol{\zeta}^*$ and $v = (\bar{\boldsymbol{\Psi}}\boldsymbol{\zeta}^*)^T \mathbf{R} \bar{\boldsymbol{\Psi}}\boldsymbol{\zeta}^*$) i.e., ρ increases monotonically with p. $\hat{\varepsilon}_m$ decreases monotonically with $\hat{n}$ as indicated by Eq. (5) [27].

Remark 1. *When the UL/DL blocklength is relatively short, increasing it results in a significant reduction in the block error rate, thereby decreasing the AoLI-FT. However, once the blocklength exceeds a certain threshold, communication latency may increase, leading to a subsequent rise in AoLI-FT. In this process, although the block error rate decreases monotonically with increasing blocklength, as indicated by Eq. (22f), the control convergence rate also increases, ultimately degrading control performance.*

However, a smaller blocklength will lead to an increased block error rate, negatively impacting the stability of the control system. Therefore, the system must find an optimal balance in blocklength to ensure optimal communication and control performance. Assuming that the UL and the DL are independent, the corresponding value of ρ can be determined according to $\hat{n}$ and $\breve{n}$. However, to find the optimal value of AoLI-FT with respect to blocklength, it is necessary to first determine the average SINR, which involves calculating its expected value. The computation of the average SINR depends on $\hat{\mathbf{w}}$ and $\breve{\mathbf{w}}$. Besides, both $\hat{n}$ and $\breve{n}$ simultaneously affect AoLI-FT.

4.1 Co-design of Communication and Control

To handle problem $\boldsymbol{Q2}$, we propose Algorithm 1, an alternative iterative search algorithm. To optimize the blocklength, which is inherently discrete, we first convert it to a real number for an approximation before reverting it to its discrete form.

In Algorithm 1, Step 1 indicates determining the search range for the UL and DL based on the given inputs, using constraints Eq. (22a) and Eq. (22b) respectively. Step 2 indicates calculating the average SINR using the Monte Carlo method with a power averaging strategy and obtaining the initial AoLI-FT.

Steps 3–11 describe the process for finding the optimal $\hat{n}$ and $\breve{n}$ while minimizing AoLI-FT. Step 4 indicates using the Golden Section method [7] to find the optimal UL blocklength $\hat{n}^*$ within the range $\hat{n}^* \in [\hat{n}_{\min}, \hat{n}_{\max}]$, while keeping the DL blocklength $\breve{n}$ fixed. Step 5 shows the concatenation of the original blocklengths and each optimized blocklength, as well as AoLI-FT. The purpose is to facilitate the selection of fixed parameters during the alternating optimization process and to determine the minimum AoLI-FT after iterative optimization. Similarly, Step 6 describes using the Golden Section algorithm to find the optimal DL blocklength $\breve{n}^*$ within the range $\breve{n}^* \in [\breve{n}_{\min}, \breve{n}_{\max}]$, while fixing the UL blocklength $\hat{n}^*$, followed by data

Algorithm 1. *The iterative search algorithm.*

Input: $\hat{n}^{(0)}$, $\breve{n}^{(0)}$, $\hat{I}$, $\breve{I}$, $P_{\max}$, M, L, Q, iterations number i_t, minimum interval n_{th};

1: Initialization: calculate $[\hat{n}_{\min}, \hat{n}_{\max}]$ and $[\breve{n}_{\min}, \breve{n}_{\max}]$;
2: Compute the averages of $\hat{\gamma}$, $\breve{\gamma}$ and $\Delta^{(0)}$ based on $P_m = \frac{P_{max}}{M}$;
3: **for** $i = 1 : i_t$ **do**
4: $\hat{n}$ = Golden section algorithm in $\breve{n}^{(0)}(i)$, $\hat{n}^* \in [\hat{n}_{\min}, \hat{n}_{\max}]$, $\hat{n}^* = \lfloor \hat{n} \rfloor$;
5: Concatenate data $\hat{n}^{(0)} = [\hat{n}^{(0)}, \hat{n}^*]$, $\Delta^{(0)} = [\Delta^{(0)}, \Delta(\hat{n}^*, \breve{n}^{(0)}(i))]$;
6: Similarly, obtain $\breve{n}^*$, $\breve{n}^{(0)}$ and $\Delta^{(0)}$ according to steps 4 and 5, respectively;
7: **if** $\left|(\hat{n}^* - \hat{n}^{(0)}(i-1))\right| \leq n_{th}$ or $\left|(\breve{n}^* - \breve{n}^{(0)}(i-1))\right| \leq n_{th}$ **then**
8: break;
9: **end if**
10: **end for**
11: $(\hat{n}^*, \breve{n}^*) = \arg\min_{\hat{n},\breve{n}} \Delta^{(0)}$ and $\rho^* = \rho(\hat{n}^*, \breve{n}^*)$;
12: **if** $\rho^* > 1$ **then**
13: $l = \text{length}(\Delta^{(0)})$, $k^* = \arg\min_{k\in[1,l]} \Delta^{(0)}$;
14: **if** $k^* < l/2$ **then**
15: $j = (k^* + 1) : l$
16: **for** j **do**
17: $b = \arg\min_{\hat{n},\breve{n}} \Delta^{(0)}(j)$;
18: **if** $2k^* - j > 1$ **then**
19: $a = \arg\min_{\hat{n},\breve{n}} \Delta^{(0)}(2k^* - j)$;
20: **else**
21: $a = \arg\min_{\hat{n},\breve{n}} \Delta^{(0)}(1)$;
22: **end if**
23: $\rho^* = \min\{\rho(a), \rho(b)\}$;
24: **if** $\rho^* < 1$ **then**
25: $(\hat{n}^*, \breve{n}^*) = \arg\min_{\hat{n},\breve{n}} \{\rho(a), \rho(b)\}$;
26: **break**;
27: **end if**
28: **end for**
29: **else**
30: Let $j = (k^* - 1) : 1$, repeat step 16 $\sim$ 28. The difference is, in step 18 $\sim$ 22, when $(j + 2) > l$, $a = \arg\min_{\hat{n},\breve{n}} \Delta^{(0)}(l)$, else $a = \arg\min_{\hat{n},\breve{n}} \Delta^{(0)}(j + 2)$;
31: **end if**
32: **end if**

Output: $\hat{n}^*$, $\breve{n}^*$, ρ^*.

concatenation. It is important to note that after data concatenation, $\hat{n}^{(0)}$ and $\breve{n}^{(0)}$ pertain only to the UL and DL blocklengths, respectively, while the $\Delta^{(0)}$ encompasses all situations. Step 7 aims to avoid repeated iterations when the optimization variable remains almost unchanged. In Step 11, the minimum value of AoLI-FT is sought to determine the corresponding optimal UL and DL blocklengths, as well as the control convergence rate.

Steps 12–32 describe the process of quickly finding the optimization variables that satisfy constraint Eq. (22e). To accelerate convergence, we use the minimum value in the AoLI-FT as the center point (Step 13), searching for results that satisfy Eq. (22e) in its neighborhood a and b, and continuously expanding to further neighborhoods. When the neighborhood value is missing, replace it with the nearest value (Step 21 and 30) until the constraint is met.

Since AoLI-FT reflects system real-time performance, minimizing AoLI-FT leads to faster transmission responses, enabling quicker system convergence. However, this does not ensure communication reliability, as it involves sacrificing communication resources to ensure optimal control performance. To meet real industrial needs, we first calculate the minimum control convergence rate $\rho_{\min}$ based on reliability. Then, we adjust Algorithm 1 so that $\rho^* < \rho_{\min}$ to achieve optimal results under reliability constraints. Reliability requirements can be balanced with control performance by appropriately adjusting the control (i.e., trading off some control performance for improved communication performance). For better adaptation to real industrial scenarios, a weighted form of AoLI-FT and reliability could be used. By adjusting the weights, the balance between communication and control systems can be optimized.

4.2 Computation Complexity

In Algorithm 1, simple arithmetic operations have a constant computational complexity of $O(1)$. Assuming the number of Monte Carlo simulations is N, the computational complexity of the SINR is $O(N)$. Considering the worst-case scenario and ignoring the computation complexity of simple arithmetic operations, in Steps 3 $\sim$ 10, the outer loop iterates i_t times, and each iteration uses the Golden Section Search algorithm to find the optimal blocklength, with complexities of $O(n_1)$ and $O(n_2)$ respectively, where n_1 and n_2 are the search interval sizes for the UL and DL blocklengths. Assuming $n_1 \geq n_2$, this part's computational complexity is $O(2i_t \log n_1)$. In Step 11, comparing the results of $2i_t + 1$ AOLI-FTs has a complexity of

Table 1. *Summary of parameters.*

Parameter	Setting value
Number of Monte Carlo similations	10^4
Number of plants M	2
Number of actuators Q	2
System matrix $\mathbf{A}_1$; $\mathbf{A}_2$	$[2,1;0,1]$; $[8,1;0,5]$
Input matrix $\mathbf{B}_1$; $\mathbf{B}_2$	$[1,0;0,1]$; $[0,1;1,0]$
Initial value $\boldsymbol{\zeta}_0$	$[7;5;1;1]$
Amount of information $\hat{\boldsymbol{I}}$; $\check{\boldsymbol{I}}$	$[200;240]$; $[200;160]$
Maximum blocklength of UL and DL $\hat{\boldsymbol{n}}_{\max}$; $\check{\boldsymbol{n}}_{\max}$	$[500;400]$; $[500;300]$
Transmit rounds $\boldsymbol{c}$	$[4;3]$
Symmetric weighting matrices $\mathbf{G}$; $\mathbf{U}$	$\boldsymbol{I}_{4\times4}$; $0.1\boldsymbol{I}_{2\times2}$
Positive definite matrix $\mathbf{R}$	$I_{4\times4}$
Number of antennas L	4
Modulation order $\hat{\Theta}$; $\check{\Theta}$	16
Total power $P_{\max}$	60 dBm
Power spectral density of noise	-174 dBm/HZ
Sample period s	20 ms

$O(2i_t)$. In Step 13, finding the position corresponding to the minimum value among $2i_t + 1$ AOLI-FTs has a complexity of $O(2i_t)$. Steps 16 $\sim$ 28 loop up to $2i_t + 1$ times, with a complexity of $O(2i_t)$. Similarly, the complexity of Step 30 is $O(2i_t)$. Summarizing all the above, the total computational complexity of Algorithm 1 is $O(N + 2i_t \log n_1 + 8i_t)$. Since $N \gg i_t$ i, the computational complexity can be simplified to $O(N)$.

For the exhaustive method, which involves finding the optimal blocklength based on the size of each element in n_1 and n_2, the computational complexity is $O(N + 2n_1^2)$. If the condition $\rho < 1$ is not met, the ρ value for each element is calculated, and the blocklength corresponding to the smallest result is chosen as the output. This has a computational complexity of $O(2n_1^2)$. Since $n_1^2 \gg N$, the overall computational complexity of the exhaustive method is $O(4n_1^2)$.

V. NUMERICAL RESULTS

Like the parameter configurations discussed in [28, 22, 16], in our work, we consider two second-order unstable and controllable physical system models, with relevant parameters shown in Table 1. We also consider Rayleigh fading channels and Gaussian noise interference, using the Monte Carlo method for multiple simulations to obtain the mean of SINR.

For the case with $M = 1$, Figure 3 illustrates the influence of blocklengths $\hat{n}$ and $\check{n}$ on the average AoLI-FT, obtained through the exhaustive search method. To better observe the effects, the range of

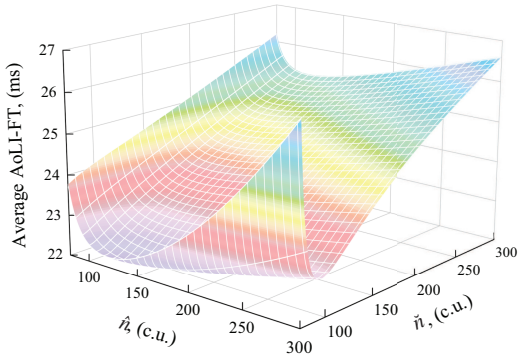

Figure 3. *The impact of $\hat{n}$ and $\check{n}$ on AoLI-FT.*

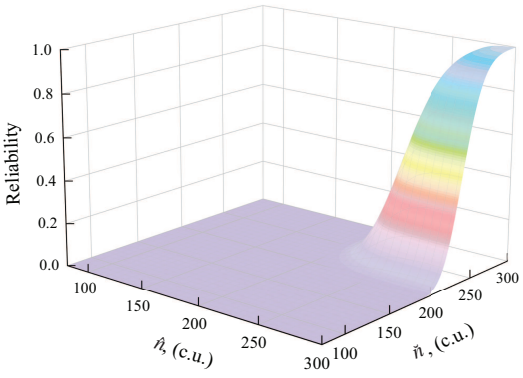

Figure 4. *The impact of $\hat{n}$ and $\check{n}$ on reliability.*

blocklengths was narrowed down to $\hat{n} = (75 : 300)$ and $\check{n} = (80 : 300)$ based on constraints. The results show the minimum average AoLI-FT is 21.45 ms at optimal blocklengths $\hat{n} = 87$ and $\check{n} = 289$. The impact of $\hat{n}$ on AoLI-FT is significant, suggesting that smaller blocklengths for the UL can reduce AoLI-FT and improve system real-time performance (even though $\hat{I}$ is large, semantic communication techniques can be applied to achieve data transmission using a smaller $\hat{n}$). However, since $\hat{\varepsilon}$ is a decreasing function of $\hat{n}$, $\hat{\varepsilon}$ is higher in this case. Conversely, the impact of $\check{n}$ is less pronounced, possibly because control commands are smaller, and setting a larger blocklength allows the recovery of the original signals through error-correcting codes even if reception fails at the actuator.

Figure 4 shows the impact of $\hat{n}$ and $\check{n}$ on reliability, demonstrating that reliability increases when both $\hat{n}$ and $\check{n}$ are large. This is consistent with theory, as the block error rate is a decreasing function of blocklength. However, higher reliability leads to a greater control convergence rate, implying a slower convergence speed and thus reduced performance of the con-

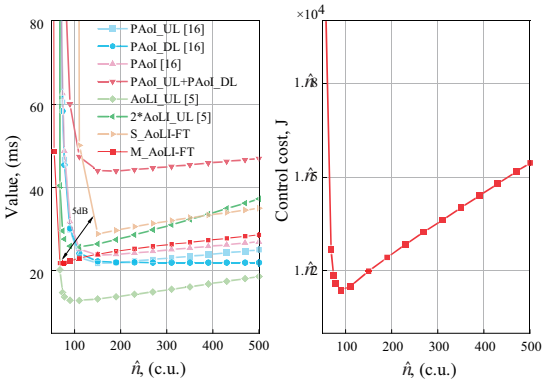

Figure 5. *Comparison of different methods. When both $\hat{n}$ and $\check{n}$ are involved, fix $\check{n} = 192$ [22].*

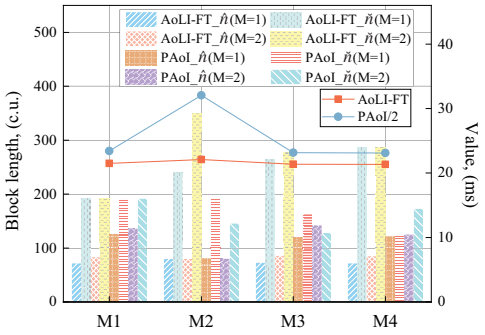

Figure 6. *Comparison of different algorithms. [22].*

trol system. Additionally, when $\hat{n}$ and $\check{n}$ are both large, the AoLI-FT increases, negatively affecting the system's real-time performance. In summary, to ensure system reliability, there may be a trade-off between system real-time performance and convergence rate. However, this can be mitigated by selecting suitable values for $\hat{n}$ and $\check{n}$, balancing the performance of these three aspects.

The left image in Figure 5 compares the proposed AoLI-FT with the new AoI measurement methods introduced in recent years. PAoI_UL represents the average peak age of information for uplink, while PAoI_DL denotes the average peak age of information for downlink, when considering them as individual wireless transmissions. PAoL refers to the average peak age of information. In our previous work, AoLI was considered when UL and DL are consistent, equivalent to the results of AoLI_UL. 2*AoLI_UL considers the total AoLI for consistent UL and DL. AoLI-FT_S results from both links having single antennas, whereas AoLI-FT_M considers multi-antenna scenarios. Compared to PAoI, the AoLI-FT_M proposed in this paper is nearly identical when considering only UL or DL. Compared to scenarios where UL and DL channels, error rates, and other parameters are identical, the minimum AoLI calculated for both links is 15.25% higher than the minimum AoLI-FT_M. Moreover, for the AoLI-FT proposed in this paper, using multiple antennas is more effective than a single antenna, increasing the average SINR by 5 dB for the system, and reducing the optimal PAoLI by 24.48%. A Comparison of the left and right images in Figure 5 reveals that as AoLI-FT increases, the control cost J also correspondingly increases. This is likely because larger AoLI-FT results in delayed updates of the control system's state information, thereby affecting the accuracy of control decisions and ultimately increasing the control cost.

Figure 6 compares the performance of different algorithms in optimizing the AoLI-FT and PAoI problems. The methods are as follows:

- M1: with $\check{n}$ fixed at 192, optimized using the Golden Section Algorithm.
- M2: with $\hat{n}$ fixed at 80, optimized using the Golden Section Algorithm.
- M3: Algorithm 1.
- M4: Exhaustive Search Method.

According to the computational complexity analysis in Section 4.2, compared to Algorithm 1 in M3, the methods in M1 and M2 only optimize the blocklengths of the UL/DL, and thus their computational complexity is consistent with that of Algorithm 1. For both the PAoI problem and AoLI-FT, Algorithm 1 not only has lower computational complexity compared to the exhaustive method but also achieves similar results. As clearly shown in the figure, the PAoI results of M2 differ significantly from the exhaustive method, indicating poor algorithm robustness. While the results of M1 are comparable to the exhaustive method, they depend on the size of the fixed values. In summary, the performance of the M2 method is superior. Additionally, in AoLI-FT, there is a significant difference in the optimal blocklengths for UL and DL, whereas in PAoI, they are almost similar. This difference arises because AoLI-FT considers flexible settings for the rounds of transmission, where DL transmissions occur after successful UL transmissions. Thus, setting a smaller block size for the UL ensures timeliness even

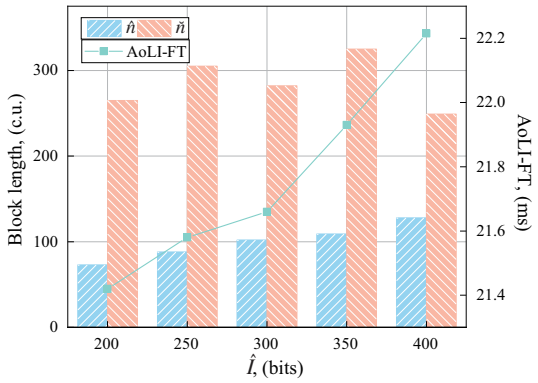

Figure 7. *Variation of $\hat{n}$, $\check{n}$, and AoLI-FT with $\hat{I}$, where $\check{I} = 200$ bits.*

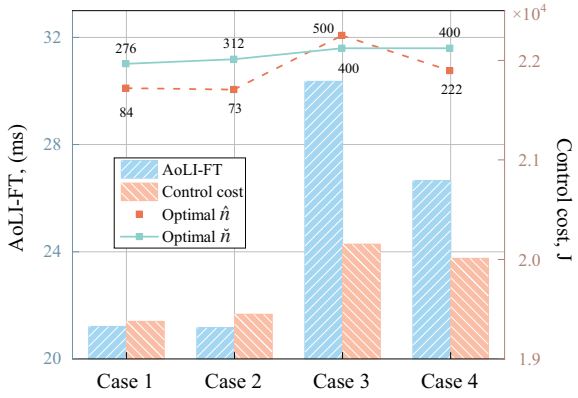

(a) *The relationship between AoLI-FT, control cost, and blocklength.*

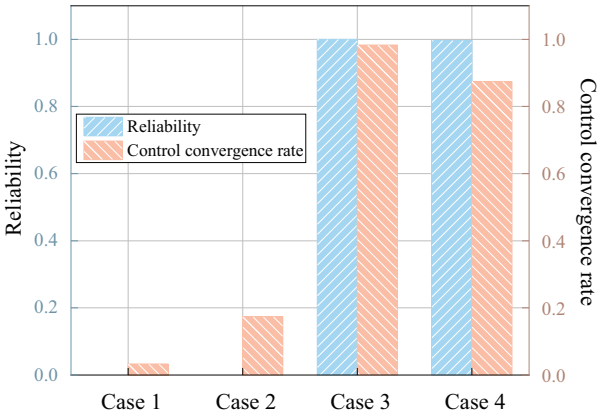

(b) *The relationship between reliability, and control convergence rate.*

Figure 8. *Performance comparison under different cases.*

after multiple retransmissions. The blocklength in the DL does not significantly impact AoLI-FT, possibly because larger block sizes allow the receiver to successfully recover the signal through error detection and correction methods, even if errors occur. While if $\check{n}$ is small, the signal can be successfully received through retransmissions.

Since the amount of data transmitted on the UL is generally less than that on the DL, Figure 7 mainly considers the scenario where $\check{I} = 200$ bits, and $\hat{I}$ is continuously increased. This analysis is based on the problem of minimizing AoLI-FT to determine $\hat{n}$ and $\check{n}$. As $\hat{I}$ increases, both $\hat{n}$ and AoLI-FT also increase continuously. Although $\hat{n}$ is small and its variation with $\hat{I}$ is minimal, its impact on AoLI-FT is significant. For example, when $\hat{I} = 200$ bits, $\hat{n} = 73$ c.u., corresponding to AoLI-FT is 21.42 ms; and when $\hat{I} = 400$ bits, $\hat{n} = 128$ c.u., corresponding to AoLI-FT is 22.22 ms (although traditionally $I/n < 1$, with the development of semantic communication technology, $I/n > 1$ is achievable). Additionally, the results indicate that setting $\check{n}$ to about three times $\hat{n}$ yields optimal AoLI-FT performance.

Figure 8 presents the optimal blocklength, average AoLI-FT, control cost, control convergence rate, and reliability results under different scenarios.

- Case 1 minimizes AoLI-FT by equally distributing power among users based on Algorithm 1.
- Case 2 minimizes AoLI-FT by allocating power proportionally according to users' AoLI-FT.
- Case 3 focuses on maximizing reliability.
- Case 4 calculates a weighted sum of AoLI-FT and reliability, with weights of 0.6 and 0.4 respectively.

The results show that Case 1 reduces transmission time by about 30% compared to Case 3 by setting smaller UL blocklength and three times larger DL blocklengths. Case 2 shows similar outcomes to Case 1 due to the similarity in subsystems considered. Although Case 3 achieves near-perfect reliability, it sacrifices time, control cost, and control convergence rate. In contrast, Case 4 balances reliability and system responsiveness, showing a control convergence rate of 0.875 and an AoLI-FT of 26.6 ms, marking 25.4% increase and 12.39% decrease compared to Cases 1 and Case 3 respectively, with control costs lying between those cases.

VI. CONCLUSION

In this paper, we propose a novel method for the co-design of communication and control system within

IIoT. Our approach introduces the AoLI-FT metric and targets the minimization of its average value. Initially, we derive an approximate expression for the upper bound of the average AoLI-FT. Next, we established a connection between the communication and control systems using a Lyapunov-like function. Subsequently, we propose an iterative alternating algorithm to minimize the average AoLI-FT, optimizing blocklength while ensuring compliance with control constraints. The numerical results indicate that our proposed design method can enhance communication real-time performance while maintaining control performance. Furthermore, depending on the system performance requirements in different scenarios, combining the iterative alternating algorithm with a weighted approach can effectively balance the overall performance of communication and control systems.

ACKNOWLEDGEMENT

The work of Tang Jianhua was supported in part by the National Key R&D Program of China under Grant 2024YFE0200500, in part by the Guangdong Basic and Applied Basic Research Foundation under Grant 2024A1515012615, and in part by the Department of Science and Technology of Guangdong Province under Grant 2021QN02X491.

NOTES

[1]Unlike the communication noise $\hat{v}_{k,m}$ (noise from the external environment during signal transmission), the process noise $\boldsymbol{v}_{k,m}$ represents the system's internal uncertainties.

APPENDIX A

In the Section 3.3, to obtain $\mathbb{E}(T) = T_s(\mathbb{E}(\hat{C})\hat{n} + \mathbb{E}(\check{C})\check{n})$, we have to find the $\mathbb{E}(\hat{C})$ and $\mathbb{E}(\check{C})$. Based on the series expansion, we can obtain the average rounds of transmissions for the UL as

$$\begin{aligned}\mathbb{E}(\hat{C}) &= \frac{\sum_{\hat{c}=1}^{c-1}\hat{c}\hat{p}^{\hat{c}-1}(1-\hat{p})}{1-\hat{p}^{c-1}} \\ &= \frac{1}{1-\hat{p}} - \frac{(c-1)\hat{p}^{c-1}}{1-\hat{p}^{c-1}},\end{aligned} \tag{23}$$

where $\hat{p} = \mathbb{E}(\hat{\varepsilon}) \approx 1 - \exp\left(-\frac{\hat{\delta}-\frac{\sqrt{\pi\hat{I}}}{\hat{n}}}{\hat{\gamma}}\right)$ represents the average error block rate for the UL [16]. Since the DL transmission occurs after the successful transmission of the UL, the total rounds of transmissions for both UL and DL is c. Therefore, the average rounds of transmissions for the DL can be expressed as

$$\begin{aligned}\mathbb{E}(\check{C}) &= \sum_{\hat{c}=1}^{c-1}\sum_{\check{c}=1}^{c-\hat{c}}\check{c}\frac{\check{p}^{\check{c}-1}(1-\check{p})}{1-\check{p}^{c-\hat{c}}}\frac{\hat{p}^{\hat{c}-1}(1-\hat{p})}{1-\hat{p}^{c-1}} \\ &= \frac{1}{1-\check{p}} + \frac{c(1-\hat{p})-(1-\hat{p}^c)}{(1-\hat{p})(1-\hat{p}^{c-1})} \\ &\quad - \frac{1-\hat{p}}{1-\hat{p}^{c-1}}\sum_{\hat{c}=1}^{c-1}(c-\hat{c})\frac{\hat{p}^{\hat{c}-1}}{1-\check{p}^{c-\hat{c}}},\end{aligned} \tag{24}$$

where $\check{p} = \mathbb{E}(\check{\varepsilon}) \approx 1 - \exp\left(-\frac{\check{\delta}-\frac{\sqrt{\pi\check{I}}}{\check{n}}}{\check{\gamma}}\right)$ represents the average error block rate for the DL.

In an actual industrial scenario, where $0 < \hat{p} < 1$, $0 < \check{p} < 1$ (for example, the reliability of discrete automatic motion control is required to be at least 99.9999% [29]), and $2 < c < \infty$. In equations Eq. (23) and Eq. (24), the subtraction terms are both greater than zero. We can obtain the upper bound of $\mathbb{E}(T)$ as

$$\mathbb{E}(\bar{T}) = \frac{T_s\hat{n}}{1-\hat{p}} + T_s\check{n}\left[\frac{1}{1-\check{p}} + \frac{c(1-\hat{p})-(1-\hat{p}^c)}{(1-\hat{p})(1-\hat{p}^{c-1})}\right]. \tag{25}$$

In actual industrial scenarios, the UL generally transmits more information. Therefore, when the total number of transmission rounds for the uplink and downlink is i, the time required for data transmission is $\bar{t}_1 = T_s(\hat{c}\hat{n} + (i-\hat{c})\check{n})$. In region A, the generation time $\bar{t}$ of two status update packages is within the range $\bar{t}_1 \le \bar{t} \le \frac{2}{\lambda}$. Utilizing the probability density function of $\bar{T}$, we can get

$$\begin{aligned}\mathbb{E}(A \mid C=i) &= \int_{\bar{t}_1}^{\frac{2}{\lambda}} \bar{t}\lambda e^{-\lambda(\bar{t}-\bar{t}_1)}d\bar{t} \\ &= \frac{1}{\lambda} + \bar{t}_1 - \frac{2}{\lambda}e^{\lambda(\bar{t}_1-\frac{2}{\lambda})} \\ &\le \frac{1}{\lambda} + \bar{t}_1.\end{aligned} \tag{26}$$

$$\begin{aligned}\mathbb{E}(A^2 \mid C=i) &= \int_{\bar{t}_1}^{\frac{2}{\lambda}} \bar{t}^2 \lambda e^{-\lambda(\bar{t}-\bar{t}_1)} d\bar{t} \\ &= \bar{t}_1^2 + \frac{2\bar{t}_1}{\lambda} + \frac{2}{\lambda^2} - \frac{10}{\lambda^2} e^{\lambda(\bar{t}_1 - \frac{2}{\lambda})} \\ &\leq \frac{2}{\lambda^2} + \frac{2\bar{t}_1}{\lambda} + \bar{t}_1^2.\end{aligned} \tag{27}$$

Substituting Eq. (26) into Eq. (15), and use the arithmetic series summation formula, we can get the upper bound of $\mathbb{E}(\bar{A})$ is

$$\begin{aligned}\mathbb{E}(\bar{A}) &= \sum_{i=2}^{c}\sum_{\hat{c}=1}^{i-1}(\frac{1}{\lambda}+\bar{t}_1)\frac{\hat{p}^{\hat{c}-1}(1-\hat{p})}{1-\hat{p}^{c-1}}\frac{\check{p}^{i-\hat{c}-1}(1-\check{p})}{1-\check{p}^{c-\hat{c}}} \\ &\approx s + T_s(\hat{n}-\check{n})(\frac{1}{1-\hat{p}} - \frac{(c-1)\hat{p}^{c-1}}{1-\hat{p}^{c-1}}) \\ &+ T_s\check{n}(\frac{1}{1-\check{p}} + \frac{1-\hat{p}}{1-\hat{p}^{c-1}}\frac{1-c\check{p}^{c-1}}{1-\check{p}^{c-1}}),\end{aligned} \tag{28}$$

where $\frac{1}{\lambda}$ is not related to the summation. Expand the summation part $\sum_{i=2}^{c}\sum_{\hat{c}=1}^{i-1}\frac{\hat{p}^{\hat{c}-1}(1-\hat{p})}{1-\hat{p}^{c-1}}\frac{\check{p}^{i-\hat{c}-1}(1-\check{p})}{1-\check{p}^{c-\hat{c}}} = \frac{1-\hat{p}}{1-\hat{p}^{c-1}}\frac{(1-\check{p})(1+\check{p}+\ldots+\check{p}^{c-2})}{1-\check{p}^{c-1}} +$ [ht] $\frac{\hat{p}(1-\hat{p})}{1-\hat{p}^{c-1}}\frac{(1-\check{p})(1+\check{p}+\ldots+\check{p}^{c-3})}{1-\check{p}^{c-2}} + \ldots + \frac{\hat{p}^{c-1}(1-\hat{p})}{1-\hat{p}^{c-1}}$. where each term can be understood as the probability of the UL transmitting only $i-1$ times multiplied by the probability of the DL transmitting $c-i$ times ($\check{c} \leq c-i$). According to the geometric series summation formula, it is easy to calculate that the result of summation part is 1. The second and third items in $*$ are calculated based on $\sum_{i=2}^{c}\sum_{\hat{c}=1}^{i-1}\hat{c}\frac{\hat{p}^{\hat{c}-1}(1-\hat{p})}{1-\hat{p}^{c-1}}\frac{\check{p}^{i-\hat{c}-1}(1-\check{p})}{1-\check{p}^{c-\hat{c}}}$ and $\sum_{i=2}^{c}\sum_{\hat{c}=1}^{i-1} i\frac{\hat{p}^{\hat{c}-1}(1-\hat{p})}{1-\hat{p}^{c-1}}\frac{\check{p}^{i-\hat{c}-1}(1-\check{p})}{1-\check{p}^{c-\hat{c}}}$, respectively. The former can be directly obtained by simplification, while the latter yields a result of $\frac{1}{1-\check{p}}+\frac{1-\hat{p}}{1-\hat{p}^{c-1}}(\frac{1-c\check{p}^{c-1}}{1-\check{p}^{c-1}}+\hat{p}\frac{2-c\check{p}^{c-2}}{1-\check{p}^{c-2}}+\ldots+\hat{p}^{c-2}\frac{(c-1)-c\check{p}}{1-\check{p}})$. Due to the generally low block error rate, $\frac{1-\hat{p}}{1-\hat{p}^{c-1}}$ is close to 1. Although $\frac{2-c\check{p}^{c-2}}{1-\check{p}^{c-2}}$ is greater than 1, it will be quite small after being multiplied by $\hat{p}$. Similarly, the terms containing higher powers of $\hat{p}$ in the parentheses will be even smaller. Therefore, the third term can be approximated as $\frac{1}{1-\check{p}} + \frac{1-\hat{p}}{1-\hat{p}^{c-1}}\frac{1-c\check{p}^{c-1}}{1-\check{p}^{c-1}}$.

Based on Eq. (28), the upper bound of $\mathbb{E}(\bar{A}^2)$ can be expressed as Eq. (29).

$$\begin{aligned}\mathbb{E}(\bar{A}^2) &= \sum_{i=2}^{c}\sum_{\hat{c}=1}^{i-1}(\frac{2}{\lambda^2}+\frac{2\bar{t}_1}{\lambda}+\bar{t}_1^2)\frac{\hat{p}^{\hat{c}-1}(1-\hat{p})}{1-\hat{p}^{c-1}}\frac{\check{p}^{i-\hat{c}-1}(1-\check{p})}{1-\check{p}^{c-\hat{c}}} \\ &\approx 2s^2 + 2s(\mathbb{E}(\bar{A})-s) + a_1T_s^2(\hat{n}-\check{n})^2 + 2\check{n}T_s^2(\hat{n}-\check{n})\underbrace{[\frac{1}{1-\check{p}}(\frac{1}{1-\hat{p}} - \frac{(c-1)\hat{p}^{c-1}}{1-\hat{p}^{c-1}}) + a_2]}_{①} \\ &+ a_3T_s^2\check{n}^2\underbrace{[\frac{1}{1-\check{p}} + \frac{3}{(1-\check{p})^2} + \frac{2\check{p}(1-\check{p}^{c-2})}{(1-\check{p})^3}]}_{②},\end{aligned} \tag{29}$$

where $a_1 = \frac{1-(2c-3)\hat{p}^{c-1}}{(1-\hat{p})(1-\hat{p}^{c-1})} + \frac{2\hat{p}}{(1-\hat{p})^2} - \frac{(c-1)^2\hat{p}^{c-1}}{1-\hat{p}^{c-1}}$ $a_2 = \frac{1-\hat{p}}{1-\hat{p}^{c-1}}\frac{1-c\check{p}^{c-1}}{1-\check{p}^{c-1}}$ and $a_3 = \frac{1-\hat{p}}{1-\hat{p}^{c-1}}\frac{1-\check{p}}{1-\check{p}^{c-1}}$. Let $\omega = \frac{\hat{p}^{\hat{c}-1}(1-\hat{p})}{1-\hat{p}^{c-1}}\frac{\check{p}^{i-\hat{c}-1}(1-\check{p})}{1-\check{p}^{c-\hat{c}}}$, then $\sum_{i=2}^{c}\sum_{\hat{c}=1}^{i-1}\bar{t}_1^2\omega$ in Eq. (29) is mainly related to $\sum_{i=2}^{c}\sum_{\hat{c}=1}^{i-1}\hat{c}^2\omega$, $\sum_{i=2}^{c}\sum_{\hat{c}=1}^{i-1}i\hat{c}\omega$ and $\sum_{i=2}^{c}\sum_{\hat{c}=1}^{i-1}i^2\omega$. Using the geometric series summation formula, it is easy to calculate that

- $\sum_{i=2}^{c}\sum_{\hat{c}=1}^{i-1}\hat{c}^2\omega = \frac{1-(2c-3)\hat{p}^{c-1}}{(1-\hat{p})(1-\hat{p}^{c-1})} + \frac{2\hat{p}(1-\hat{p}^{c-2})}{(1-\hat{p})^2(1-\hat{p}^{c-1})} - \frac{(c-1)^2\hat{p}^{c-1}}{1-\hat{p}^{c-1}}$. In actual industrial scenarios, $\frac{1-\hat{p}^{c-2}}{1-\hat{p}^{c-1}} \approx 1$, therefore, $\sum_{i=2}^{c}\sum_{\hat{c}=1}^{i-1}\hat{c}^2\omega$ can be approximated as a_1.

- $\sum_{i=2}^{c}\sum_{\hat{c}=1}^{i-1}i\hat{c}\omega = \frac{1}{1-\check{p}}(\frac{1}{1-\hat{p}} - \frac{(c-1)\hat{p}^{c-1}}{1-\hat{p}^{c-1}}) + \frac{1-\hat{p}}{1-\hat{p}^{c-1}}[\frac{1-c\check{p}^{c-1}}{1-\check{p}^{c-1}} + 2\hat{p}\frac{2-c\check{p}^{c-2}}{1-\check{p}^{c-2}} + \ldots + (c-1)\hat{p}^{c-2}\frac{(c-1)-c\check{p}}{1-\check{p}}]$. Where $\frac{2-c\check{p}^{c-2}}{1-\check{p}^{c-2}} = \frac{1}{1-\check{p}^{c-2}} + \frac{1-c\check{p}^{c-2}}{1-\check{p}^{c-2}} \approx 2$, the smaller $\check{p}$ is and the larger c becomes, the closer it approaches. Therefore, $[\cdot] = [1+2^2\hat{p}^2+\ldots+(c-1)^2\hat{p}c-2]$, and $\sum_{i=2}^{c}\sum_{\hat{c}=1}^{i-1}i\hat{c}\omega$ can be approximated as ①.

- $\sum_{i=2}^{c}\sum_{\hat{c}=1}^{i-1}i^2\omega = a_3(\frac{2^2-c^2\check{p}^{c-1}}{1-\check{p}} + \frac{3\check{p}-(2c-1)\check{p}^{c-1}}{(1-\check{p})^2} + \frac{2\check{p}(1-\check{p}^{c-2})}{(1-\check{p})^3}) + a_3\hat{p}(\frac{3^2-c^2\check{p}^{c-2}}{1-\check{p}} + \frac{5\check{p}-(2c-1)\check{p}^{c-2}}{(1-\check{p})^2} + \frac{2\check{p}(1-\check{p}^{c-3})}{(1-\check{p})^3}) + \ldots + a_3\hat{p}^{c-2}(\frac{c^2-c^2\check{p}}{1-\check{p}} + \frac{(2c-1))\check{p}-(2c-1)\check{p}}{(1-\check{p})^2} + \frac{2\check{p}(1-\check{p}^{c-c})}{(1-\check{p})^3})$. Since $\hat{p}$ is very small, therefore, we only retain the first product term in the above expression, and

in this product term, $(\cdot)$ is approximately equal to ②.

By substituting Eq. (25), Eq. (28), Eq. (29) into Eq. (13), the average AoLI-FT of a plant can be calculated.

References

[1] S. Vitturi, C. Zunino, *et al.*, "Industrial communication systems and their future challenges: Next-generation ethernet, iiot, and 5g," *Proceedings of the IEEE*, 2019, vol. 107, no. 6, pp. 944–961.

[2] Z. Wang, R. Liu, *et al.*, "Qos-oriented sensing–communication–control co-design for uav-enabled positioning," *IEEE Transactions on Green Communications and Networking*, 2023, vol. 7, no. 1, pp. 497–511.

[3] Y. Qiao, Y. Fu, *et al.*, "Communication–control co-design in wireless networks: A cloud control agv example," *IEEE Internet of Things Journal*, 2022, vol. 10, no. 3, pp. 2346–2359.

[4] Z. Han, X. Li, *et al.*, "Wireless communication and control co-design for system identification," *IEEE Transactions on Wireless Communications*, 2023.

[5] K. Gatsis, H. Hassani, *et al.*, "Latency-reliability tradeoffs for state estimation," *IEEE Transactions on Automatic Control*, 2020, vol. 66, no. 3, pp. 1009–1023.

[6] V. S. Varma, A. M. de Oliveira, *et al.*, "Energy-efficient time-triggered communication policies for wireless networked control systems," *IEEE Transactions on Automatic Control*, 2019, vol. 65, no. 10, pp. 4324–4331.

[7] F. Chen and J. Tang, "Co-design of communication and control based on age of loop information in industrial iot," in *IEEE Int. Conf. Commun. Technol.*, 2023, pp. 896–902.

[8] B. Chang, L. Zhang, *et al.*, "Optimizing resource allocation in urllc for real-time wireless control systems," *IEEE Transactions on Vehicular Technology*, 2019, vol. 68, no. 9, pp. 8916–8927.

[9] X. Wang, C. Chen, *et al.*, "Aoi-aware control and communication co-design for industrial iot systems," *IEEE Internet of Things Journal*, 2020, vol. 8, no. 10, pp. 8464–8473.

[10] J. Li, S. Khosravirad, *et al.*, "Communication and control interfacing for co-design of wireless control systems," in *2023 IEEE 97th Vehicular Technology Conference (VTC2023-Spring)*, 2023, pp. 1–5.

[11] D. Baumann, F. Mager, *et al.*, "Control-guided communication: Efficient resource arbitration and allocation in multi-hop wireless control systems," *IEEE Control Systems Letters*, 2019, vol. 4, no. 1, pp. 127–132.

[12] J. Li, J. Tang, *et al.*, "On the data freshness for industrial internet of things with mobile-edge computing," *IEEE Internet of Things Journal*, 2022, vol. 9, no. 15, pp. 13 542–13 554.

[13] J. Li, J. Tang, *et al.*, "Deep reinforcement learning for data freshness-oriented scheduling in industrial iot," in *GLOBECOM 2022-2022 IEEE Global Communications Conference*, 2022, pp. 6271–6276.

[14] A. M. Girgis, J. Park, *et al.*, "Predictive control and communication co-design via two-way gaussian process regression and aoi-aware scheduling," *IEEE Transactions on Communications*, 2021, vol. 69, no. 10, pp. 7077–7093.

[15] B. Chang, B. Kizilkaya, *et al.*, "Effective age of information in real-time wireless feedback control systems," *Science China Information Sciences*, 2021, vol. 64, pp. 1–14.

[16] B. Yu, Y. Cai, *et al.*, "Average age of information in short packet based machine type communication," *IEEE Transactions on Vehicular Technology*, 2020, vol. 69, no. 9, pp. 10 306–10 319.

[17] C. Vahapoglu, T. J. O'Shea, *et al.*, "Deep learning based uplink multi-user simo beamforming design," *arXiv preprint arXiv:2309.16603*, 2023.

[18] J. Jee, G. Kwon, *et al.*, "Precoding design and power control for sinr maximization of miso system with nonlinear power amplifiers," *IEEE Transactions on Vehicular Technology*, 2020, vol. 69, no. 11, pp. 14 019–14 024.

[19] B. Makki, T. Svensson, *et al.*, "Finite block-length analysis of spectrum sharing networks using rate adaptation," *IEEE Transactions on Communications*, 2015, vol. 63, no. 8, pp. 2823–2835.

[20] K. Gatsis, M. Pajic, *et al.*, "Opportunistic control over shared wireless channels," *IEEE Transactions on Automatic Control*, 2015, vol. 60, no. 12, pp. 3140–3155.

[21] C. Chen, L. Lyu, *et al.*, "On-demand transmission for edge-assisted remote control in industrial network systems," *IEEE Transactions on Industrial Informatics*, 2019, vol. 16, no. 7, pp. 4842–4854.

[22] J. Cao, X. Zhu, *et al.*, "Age of loop for wireless networked control system in the finite blocklength regime: Average, variance and outage probability," *IEEE Transactions on Wireless Communications*, 2023.

[23] W. Ding and M. Shikh-Bahaei, "Optimized asymmetric feedback detection for rate-adaptive harq with unreliable feedback," in *Proc. IEEE Wireless Commun. Netw. Conf. (WCNC)*, 2021, pp. 1–6.

[24] J. Tang, F. Chen, *et al.*, "Learn to schedule: Data freshness-oriented intelligent scheduling in industrial iot," *IEEE Trans. Cognit. Commun. Networking*, 2024.

[25] R. Long, Y. Liang, *et al.*, "Active intelligent reflecting surface for simo communications," in *Proc. IEEE GLOBECOM*, 2020, pp. 1–6.

[26] X. Wang, P. Zhu, *et al.*, "Pilot-assisted simo-noma signal detection with learnable successive interference cancellation," *IEEE Communications Letters*, 2021, vol. 25, no. 7, pp. 2385–2389.

[27] J. Cao, X. Zhu, *et al.*, "Joint block length and pilot length optimization for urllc in the finite block length regime," in *2019 IEEE Global Communications Conference (GLOBECOM)*, 2019, pp. 1–6.

[28] J. Cao, X. Zhu, *et al.*, "Age of loop oriented wireless networked control system: Communication and control co-design in the fbl regime," in *IEEE INFOCOM 2022-IEEE Conference on Computer Communications Workshops (INFOCOM WKSHPS)*, 2022, pp. 1–6.

[29] S. Wang, J. Wang, *et al.*, "Development of deterministic networking techniques for industrial manufacturing," *Strategic Study of Chinese Academy of Engineering*, 2021, vol. 23, no. 2, pp. 22–29.

Biographies

Chen Fangfang received the bachelor's degree from School of Information Science and Engineering, Xinjiang University, Xinjiang, China, in 2019, and received the master's degree from School of Information Science and Engineering, Xinjiang University, Xinjiang, China, in 2022. She is currently pursuing towards the doctor's degree with the Shien-Ming Wu School of Intelligent Engineering, South China University of Technology, Guangzhou, China. Her research interests include co-design of communication and control, semantic communication and industrial Internet of Things.

Tang Jianhua received the B.E. degree in communications engineering from Northeastern University, China, in 2010, and the Ph.D degree in electrical and electronic engineering from Nanyang Technological University, Singapore, in 2015. He was a Post-Doctoral Research Fellow with the Singapore University of Technology and Design from 2015 to 2016, and a Research Assistant Professor with the Department of Electrical and Computer Engineering, Seoul National University, South Korea, from 2016 to 2018. He is currently an Associate Professor with the Shien-Ming Wu School of Intelligent Engineering, South China University of Technology, China. His research interests include wireless communications, edge computing, network slicing and industrial Internet of Things. He was honored with the 2020 IEEE Communications Society Stephen O. Rice Prize and the 2023 IEEE ICCT Best Paper Award. He is currently serving as an Editor for the *IEEE Wireless Communications Letters* and *Digital Communications and Networks*.

Yin Zihang received the B.E. degree from Chongqing University, Chongqing, China, in 2015, and the master's degree from China Aerospace Science and Technology Corporation (CASC) 9th Academy 771 Research Institute, Xi'an, China, in 2018. He is currently a Researcher with the Research Institute of Industrial Internet of Things, China Academy of Information and Communications Technology, Beijing, China. His research focuses on Industrial Internet of Things Identity Carriers, Blockchain System Design, Artificial Intelligence Edge Computing System Design and solid-state drive (SSD) Software Algorithm Design.